17èmes JOURNEES DE L'HYDRODYNAMIQUE
JH2020

24 - 26 novembre 2020
CHERBOURG - en - COTENTIN

# MULTI-PHASE SWENSE METHOD BASED ON THE LEVEL-SET INTERFACE MODELLING

*17emes JOURNEES DE L'HYDRODYNAMIQUE JH2020*

**Y.-M. Choi[1, 2]*, B. Bouscasse[2], L. Gentaz[2], P. Ferrant[2], S. Seng[1], and Š. Malenica[1]**

[1]Research Department, Bureau Veritas, Paris, France
[2]LHEEA, CNRS UMR 6598, École Centrale de Nantes, Nantes, France
*Corresponding author: youngmyung.choi@bureauveritas.com

**Résumé**

Dans le cadre de la problématique de l'interaction onde-structure, un modèle d'écoulement multi-phase basé sur la méthode SWENSE (Spectral Wave Explicit Navier-Stokes Equations) est proposé avec une interface air-eau représentée par une fonction Level-Set. Les champs de vitesse, pression et la fonction Level-Set sont décomposés en parties incidente et complémentaire. Les termes incidents correspondant aux équations d'Euler sont annulés grace à une extrapolation de la pression incidente dans la zone d'air. La vitesse et pression incidente sont étendues dans la zone d'air avec des polynomiales cubiques pour avoir une transition progressive et des valeurs réalistes. Des études paramétriques sont réalisées sur le modèle proposé et les simulations sur un cylindre circulaire d'axe verticale dans la vague régulière sont établies et donnent des résultats satisfaisants.

**Summary**

The multi-phase flow based on the SWENSE (Spectral Wave Explicit Navier-Stokes Equations) method with Level-Set function for modeling the interface is proposed for the wave-structure interaction problem. The fluid velocity, pressure and level-set function are decomposed into the incident and complementary parts. Part of the incident terms associated with Euler equations are canceled by introducing in air an extrapolated incident pressure by density. The incident velocity and pressure are extended up to the air region by using cubic polynomials to have smooth transition and realistic values. A series of parametric studies on the proposed model is performed. A benchmark test on a vertical circular cylinder in regular waves is conducted and obtained force-harmonics show competitive results.

## 1. Introduction

The viscous flow model based on finite volume discretization for the wave-structure interaction problem is now commonly used as sufficient computational resources are accessible. Highly nonlinear phenomena such as wave breaking, wave impact, and the effect of viscosity and vorticity can be modeled easily. The interface between air and water can be modeled by introducing a color function. The commonly used color functions

are Volume Of Fluid (VOF), Level-Set (LS) Function or Phase Function (PF) [1, 2, 3]. The behavior of the interface is determined by solving the transport equation of the color function. The convection terms in the transport equation introduce the numerical damping which causes interface smearing, and controlling the quality of wave propagation in the computational domain becomes important. Many techniques to keep the interface sharp and to have less dissipation have been proposed [4, 5, 6].

Ferrant et al. (2003) introduced a functional decomposition method which is named as Spectral Wave Explicit Navier-Stokes Equations (SWENSE) not to consider the incident waves in the variable to solve [7]. It decomposes the total functional quantity into the incident and complementary parts. As the incident flow is assumed to be known, the governing equations are reformulated for the complementary terms. If the fully nonlinear potential flow model is used for incident waves, some of the incident terms associated with the Euler equations can be eliminated. Therefore, the numerical model concerns only the complementary parts. It makes the computational grid to be modeled dense near to the body only and is regarded as efficient. This methodology has been applied for single-phase fluids by [8, 9, 10] with marine hydrodynamic purposes. Recently, the principles of SWENSE have been extended to the multi-phase flow. The decomposition of velocity and LS function is applied by [11]. Li (2018) decomposed the velocity and pressure, then the Euler terms are eliminated by introducing the pseudo incident pressure [12].

In the present study, the velocity, pressure and LS fields are decomposed into the incident and complementary parts and the terms associated with the Euler equations are canceled. A parametric study on the proposed model is conducted for wave propagation with a periodic boundary. Finally, benchmark tests on a vertical circular cylinder in regular waves are conducted.

## 2. Theoretical background

2.1 Navier-Stokes equations for multi-phase flow

Incompressible air and water which has an interface between two fluids are considered in the present study. The behavior of fluid is governed by the Navier-Stokes equations given as:

$$\begin{aligned} \nabla \cdot \mathbf{u}_i &= 0 \\ \frac{\partial \mathbf{u}_i}{\partial t} + \nabla \cdot (\mathbf{u}_i \mathbf{u}_i) &= -\frac{1}{\rho_i} \nabla p_i + \nabla \cdot \left( \nu_i \left( \nabla \mathbf{u}_i + \nabla \mathbf{u}_i^T \right) \right) + \mathbf{g} \qquad i = a \quad \text{or} \quad w \end{aligned} \tag{1}$$

where subscripts $i = a, w$ represent the quantities associated with air ($_a$) and water ($_w$), respectively. The fluid density $\rho$ and the kinematic viscosity $\nu$ are characterized by fluid. $\mathbf{u}$, $p$ and $\mathbf{g}$ are the fluid velocity, pressure and gravitational acceleration, respectively.

On the interface, two conditions are imposed. The kinematic condition states that air and water particles on the interface move together and it is given in:

$$\mathbf{u}_a = \mathbf{u}_w \qquad \Leftrightarrow \qquad [\![\mathbf{u}]\!] = \mathbf{u}_a - \mathbf{u}_w = 0 \qquad \mathbf{x} \in S_F \tag{2}$$

where the jump operator $[\![f]\!] = f_a - f_w$ is defined hereafter to represent the difference of quantity $f$ across the interface $S_F$. The other interface condition is called the dynamic condition. It states about the stress balance on the interface [13, 14] which gives the tangential and normal stress balance. With a dimensional analysis on the stress balance Huang et al. (2007) showed that the tangential stress balance, effect of viscosity and surface tension can be neglected in a marine application which is characterized by a high Reynolds number [15]. The dynamic condition for a high Reynolds number is simply given as:

$$p_w = p_a \qquad \Leftrightarrow \qquad [\![p]\!] = 0 \qquad \mathbf{x} \in S_F \tag{3}$$

The Level-Set (LS) function introduced for interface modeling is defined as the signed distance function

from the interface:

$$\psi(\mathbf{x}) = \begin{cases} -d & \text{if} \quad \mathbf{x} \in \Omega_a \\ 0 & \text{if} \quad \mathbf{x} \in S_f \\ d & \text{if} \quad \mathbf{x} \in \Omega_w \end{cases} \tag{4}$$

where $d$ is the distance from the interface $S_F$, and $\Omega_a$ and $\Omega_w$ represent the air and water region, respectively. The interface is determined by solving the transport equation of LS function given in

$$\frac{\partial \psi}{\partial t} + \mathbf{u} \cdot \nabla \psi = 0 \tag{5}$$

As the LS function can represent the air and water by its signed value, the air and water can be accounted as the mixture as:

$$\begin{aligned} \rho &= \alpha \rho_w + (1-\alpha)\rho_a \\ \nu &= \alpha \nu_w + (1-\alpha)\nu_a \end{aligned} \tag{6}$$

with the Volume Of Fluid (VOF; $\alpha$) :

$$\alpha = \frac{1}{2}\left[\{\text{sign}\psi(\mathbf{x})\} + 1\right] \tag{7}$$

The Navier-Stokes equations for air and water in (1) can be written as combined equations for the mixture as

$$\nabla \cdot \mathbf{u} = 0 \tag{8a}$$

$$\frac{\partial \mathbf{u}}{\partial t} + \nabla \cdot (\mathbf{u}\mathbf{u}) = -\frac{1}{\rho}\nabla p + \nabla \cdot \left(\nu \left(\nabla \mathbf{u} + \nabla \mathbf{u}^T\right)\right) + \mathbf{g} \tag{8b}$$

## 2.2 SWENSE for multi-phase flow

The Spectral Wave Explicit Navier-Stokes Equations (SWENSE) method has been introduced for the wave-structure interaction problem by [7]. The main principle of SWENSE deals with the decomposition of functional quantity $\chi$ into the incident and complementary parts:

$$\chi = \chi_I + \chi_C \tag{9}$$

where the subscripts $_I$ and $_C$ represent the incident and complementary quantities, respectively. As the incident quantity, which is available from the potential flow model, can satisfy the Euler equations if the incident wave model, satisfying the fully nonlinear free surface condition, is used, some terms associated in the Euler equations can be canceled. Then, unknowns are the complementary parts only which are zero when the body does not exist. The SWENSE method has been validated for several marine applications as described in [8, 9, 10]. Recently, the principle of SWENSE has been extended to the multi-phase flow. Vukčević et al. (2016) have adopted the velocity and LS function decomposition but the total pressure remains in the governing equations, e.g. terms associated with the Euler equations are not canceled [11]. Later Li (2018) decomposed the fluid velocity and pressure by introducing a pseudo incident pressure and terms associated with the Euler equations can be eliminated [12]. Nevertheless the interface quantity is not decomposed as he adopted the VOF function for the interface modeling. In the present study, ideas of two previous studies are combined to decompose the fluid velocity, pressure and LS function as

$$\mathbf{u} = \mathbf{u}_I + \mathbf{u}_C \quad \Leftrightarrow \quad \mathbf{u}_C = \mathbf{u} - \mathbf{u}_I \tag{10a}$$

$$p = p_I + p_C \quad \Leftrightarrow \quad p_C = p - p_I \tag{10b}$$

$$\psi = \psi_I + \psi_C \quad \Leftrightarrow \quad \psi_C = \psi - \psi_I \tag{10c}$$

To eliminate the terms associated with Euler equations for the mixture, a pseudo incident pressure, which is scaled with the mixture density, is introduced as [12]:

$$p_I^* = \frac{\rho}{\rho_w} p_I \tag{11}$$

Then, the Euler equations for the incident flow can be expressed as:

$$\frac{\partial \mathbf{u}_I}{\partial t} + \nabla \cdot (\mathbf{u}_I \mathbf{u}_I) = -\frac{1}{\rho} \nabla p_I^* + \frac{p_I}{\rho_w} \frac{\nabla \rho}{\rho} + \mathbf{g} \tag{12}$$

The second term in the right-hand-side, $\frac{p_I}{\rho_w}\frac{\nabla \rho}{\rho}$ is equal to zero in both water and air regions, respectively, but it has non-zero value on the interface $S_F$. Substituting (10) into equations (8) and (5), and using the relations $\nabla \cdot \mathbf{u}_I = 0$ and (12), we obtain the SWENSE equations for multi-phase flow based on LS function:

$$\nabla \cdot \mathbf{u}_C = 0 \tag{13a}$$

$$\frac{\partial \mathbf{u}_C}{\partial t} + \nabla \cdot (\mathbf{u}\mathbf{u}_C) + \mathbf{u}_C \cdot \nabla \mathbf{u}_I = -\frac{1}{\rho} \nabla p_c - \frac{p_I}{\rho_w} \frac{\nabla \rho}{\rho} + \nabla \cdot \left[ \nu \left( \nabla \mathbf{u}_C + \nabla \mathbf{u}_C^T \right) \right] \tag{13b}$$

$$\frac{\partial \psi_C}{\partial t} + \mathbf{u} \cdot \nabla \psi_C = -\frac{\partial \psi_I}{\partial t} - \mathbf{u} \cdot \nabla \psi_I \tag{13c}$$

The kinematic and dynamic interface conditions for complementary flow are given as:

$$[\![\mathbf{u}_C]\!] = \mathbf{u}_{C,a} - \mathbf{u}_{C,w} = 0 \tag{14a}$$

$$[\![p_C]\!] = p_{C,a} - p_{C,w} = p_I \frac{\rho_w - \rho_a}{\rho_w} = \mathscr{H}_I \tag{14b}$$

At the initial time $t = 0$, there is no disturbance due to interaction between structure and waves, the complementary velocity, pressure and LS function are set to zero as:

$$\mathbf{u}_C = 0 \qquad p_C = 0 \qquad \psi_C = 0 \qquad \text{at} \qquad t = 0 \tag{15}$$

The boundary conditions for the body and bottom surface are given as:

$$\mathbf{u}_C = \mathbf{u}_b - \mathbf{u}_I \qquad \text{and} \qquad \frac{\partial \psi_C}{\partial n} = 0 \tag{16a}$$

where $\mathbf{u}_b$ is the instantaneous velocity of the body/bottom surface. The above conditions state that no flux and LS flux across the body/bottom surface. In the far-field, the relaxation scheme is applied to absorb the complementary flow as [16]

$$\mathbf{u}_C = (1-w)\mathbf{u}_C \qquad \text{and} \qquad \psi_C = (1-w)\psi_C \tag{17a}$$

where $w \in [0,1]$ is the weight function defined in the relaxation zone, e.g. $w = 0$ at the entrance and $w = 1$ at the end of relaxation zone. Therefore, the complementary flow is set to zero at the end of the relaxation zone. The pressure boundary condition is automatically given from the extrapolated $\mathbf{u}_C$ at the boundary surface. The atmospheric boundary condition is imposed on the boundary surface at the top.

### 2.3 Modeling of incident waves

The solutions of SWENSE strongly depend on incident quantities as some terms are canceled in the Euler terms and the other terms act as the sources in momentum equations and at the boundary surface. In the present study, the incident quantities are obtained from the nonlinear potential flow model such as stream function theory for regular waves [17, 18]. As the fully nonlinear potential flow theory is limited to the water

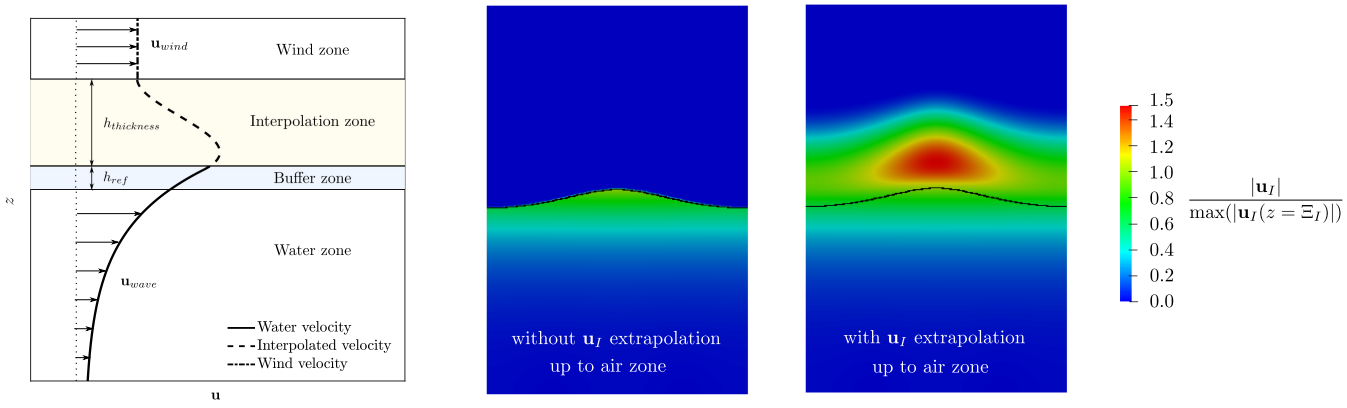


(a) Schematic view on the extension (b) $|\mathbf{u}_C|$ field with cubic polynomials extension

Figure 1. Extended incident velocity up to the air by using cubic polynomials

region, the incident flow quantities in the air are obtained by stretching the vertical modal function. The vertical modal function, which is used in the incident wave model, is given by hyperbolic function which makes the incident quantities in the air very large which is unrealistic and causes numerical instability.

In the present study, the incident velocity and pressure are extended to the air by using cubic polynomials to prevent large and unrealistic values, but to have a smooth transition from the water to the air. Let the vertical position of incident wave is at $z = \Xi$ and the incident/air quantity and its gradient are known at $z = \Xi + h_{ref}$ and $z = \Xi + h_{ref} + h_{thickness}$ as:

$$f(\Xi + h_{ref}) = f_0, \qquad \frac{df(\Xi + h_{ref})}{dz} = f_0', \tag{18a}$$

$$f(\Xi + h_{ref} + h_{thickness}) = f_1 \qquad \frac{df(\Xi + h_{ref} + h_{thickness})}{dz} = f_1'. \tag{18b}$$

where $h_{ref}$ is a reference height from the interface to the starting point of transition, $h_{thickness}$ is an interval of transition, respectively. Introducing cubic polynomials with a normalized coordinate $\tilde{\zeta}$ defined in transition interval as:

$$g(\tilde{\zeta}) = a\tilde{\zeta}^3 + b\tilde{\zeta}^2 + c\tilde{\zeta} + d, \tag{19}$$

where $a$, $b$, $c$ and $d$ are polynomial coefficients. The normalized coordinate $\tilde{\zeta} \in [0, 1]$ is obtained by:

$$\tilde{\zeta} = \frac{z - \Xi + h_{ref}}{h_{thickness}}. \tag{20}$$

The schematic view and the extended incident velocity up to the air region are shown in Figure 1.

## 3. Numerical modeling

### 3.1 Finite Volume (FV) discretization

The governing equations can be discretized with a set of collocated Finite Volume (FV) in the computational domain. The code is developed in OpenFOAM framework based on the procedure proposed by [19, 20]. The discretization is conducted with the second-order accuracy on an arbitrary polyhedral [21]. Following the discretization notation proposed by [22], the momentum equations in (13b) without pressure gradient can be discretized as

$$\left\{ \frac{\partial \mathbf{u}_C}{\partial t} + \nabla \cdot (\mathbf{u}\mathbf{u}_C) - \nabla \cdot (\nu \nabla \mathbf{u}_C) \right\}^i = \left\{ -\frac{p_I}{\rho_w} \frac{\nabla \rho}{\rho} - \mathbf{u}_C \cdot \nabla \mathbf{u}_I + \nabla \mathbf{u}_C \cdot \nabla \nu \right\}^e \tag{21}$$

where superscripts $^i$ and $^e$ represent the implicit and explicit discretization, respectively. As a result, we obtain the discretized momentum equations:

$$a_P(\mathbf{u}_C)_P + \sum_f a_N(\mathbf{u}_C)_N = \mathbf{s}(\mathbf{u}_C) \tag{22}$$

where $(q)_P$ and $(q)_N$ denote the cell-averaged value $q$ at owner $P$ and neighbor $N$ cells, respectively. $a_P$ and $a_N$ are the diagonal and off-diagonal terms of discretized momentum equations, $f$ denotes the face surface which is shared by owner and neighbor cells, $\mathbf{s}(\mathbf{u}_C)$ denotes the source terms of momentum equations, respectively. The predicted complementary velocity from the discretized momentum equation in (22) is given as:

$$(\mathbf{u}_C)'_P = \frac{1}{a_P}\mathbf{H}\{(\mathbf{u}_C)_P\} = -\frac{1}{a_P}\left\{\sum_f a_N(\mathbf{u}_C)_N - \mathbf{s}_{\mathbf{u}_C}\right\} \tag{23}$$

As the predicted complementary velocity $(\mathbf{u}_C)'_P$ do not satisfy the continuity equation, the pressure equation can be constructed to satisfy the continuity equation as:

$$\sum_f \overline{\left(\frac{1}{a_P}\right)}_f \left(\frac{1}{\rho}\nabla(p_C)_P\right)_f \cdot d\mathbf{s}_f = \sum_f \overline{\left(\frac{1}{a_P}\mathbf{H}\{(\mathbf{u}_C)_P\}\right)}_f \cdot d\mathbf{s}_f \tag{24}$$

where $\overline{(q)}_f$ is the interpolated value at the face center $f$. After solving the pressure equation, the complementary flux at face $f$ is computed as:

$$F_f = \mathbf{s}_f \cdot (\mathbf{u}_C + \mathbf{u}_I)_f = \mathbf{s}_f \cdot \left\{\overline{\left(\frac{1}{a_P}\mathbf{H}\{(\mathbf{u}_C)_P\}\right)}_f - \overline{\left(\frac{1}{a_P}\right)}_f \left(\frac{1}{\rho}\nabla(p_C)_P\right)_f + (\mathbf{u}_I)_f\right\} \tag{25}$$

### 3.2 Ghost Fluid Method(GFM) for the pressure extrapolation

The complementary pressure on the interface has a jump condition given in (14b) which requires the extrapolated pressure across the interface. The continuous fluid acceleration on the interface is given in

$$\left[\!\left[\frac{D\mathbf{u}}{Dt}\right]\!\right] = \left[\!\left[-\frac{1}{\rho}\nabla p + \nabla\cdot(\nu\nabla\mathbf{u}) + \nabla\mathbf{u}\cdot\nabla\nu + \mathbf{g}\right]\!\right] = 0, \qquad \text{on} \qquad \mathbf{x}\in S_F \tag{26}$$

For a high Reynolds number flow, the terms associated with viscosity and surface tension can be neglected. Furthermore the pseudo-incident pressure $\frac{1}{\rho}\nabla p_I$ is continuous across the interface [12], therefore the interface condition for complementary pressure gradient can be given as:

$$[\![\frac{1}{\rho}\nabla p_C]\!] = 0 \tag{27}$$

By using this relation, the complementary pressure can be extrapolated. The extrapolation procedure proposed by [11] considering jump conditions in (14b) and (27) are used in the present study. The extrapolated complementary pressure at the Ghost Fluid Cell are given as:

$$\begin{cases} (p_{C,w})_N^{GC} = \dfrac{\rho_a}{\tilde{\rho}_w}(p_C)_N + \left(1-\dfrac{\rho_w}{\tilde{\rho}_w}\right)(p_C)_P - \dfrac{\mathscr{H}_I}{\tilde{\rho}_w} & P \text{ is wet, } N \text{ is dry} \\ (p_{C,a})_N^{GC} = \dfrac{\rho_w}{\tilde{\rho}_a}(p_C)_N + \left(1-\dfrac{\rho_a}{\tilde{\rho}_a}\right)(p_C)_P + \dfrac{\mathscr{H}_I}{\tilde{\rho}_a} & P \text{ is dry, } N \text{ is wet} \end{cases} \tag{28}$$

with the interpolated density $\tilde{\rho}_w = \lambda_f\rho_w + (1-\lambda_f)\rho_a$ and $\tilde{\rho}_a = \lambda_f\rho_a + (1-\lambda_f)\rho_w$ with the normalized distance from the cell center to the interface $\lambda_f = \frac{(\psi)_P}{(\psi)_P-(\psi)_N}$. The extrapolation procedure is well described in [20].

## 4. Results and Discussion

4.1 Wave propagation with periodic boundary

The propagation of waves with periodic boundary conditions is used for the parametric study. The schematic view of the problem is shown in Figure 2. The computational domain is one wavelength ($1\lambda$) long and the height is taken to be $2h$ ($h = 0.6m$; water depth). Horizontally, the computational cells are uniformly distributed. Vertically, the cells are distributed uniformly in the free surface zone $z \in [-H, H]$ ($H$: wave height). In the water and air zones where $z \in [-h, -H], z \in [H, h]$, the cell height is gradually stretched as it goes far from the mean free surface $z = 0$ with a constant cell height ratio, $\max(\Delta z_i)/\min(\Delta z_i) = 5$ where $i$ denotes the index in vertical direction. Fully nonlinear regular wave potential solution is considered and the wave condition is given in Table 1. The same case has been used in [23] without the SWENSE model.

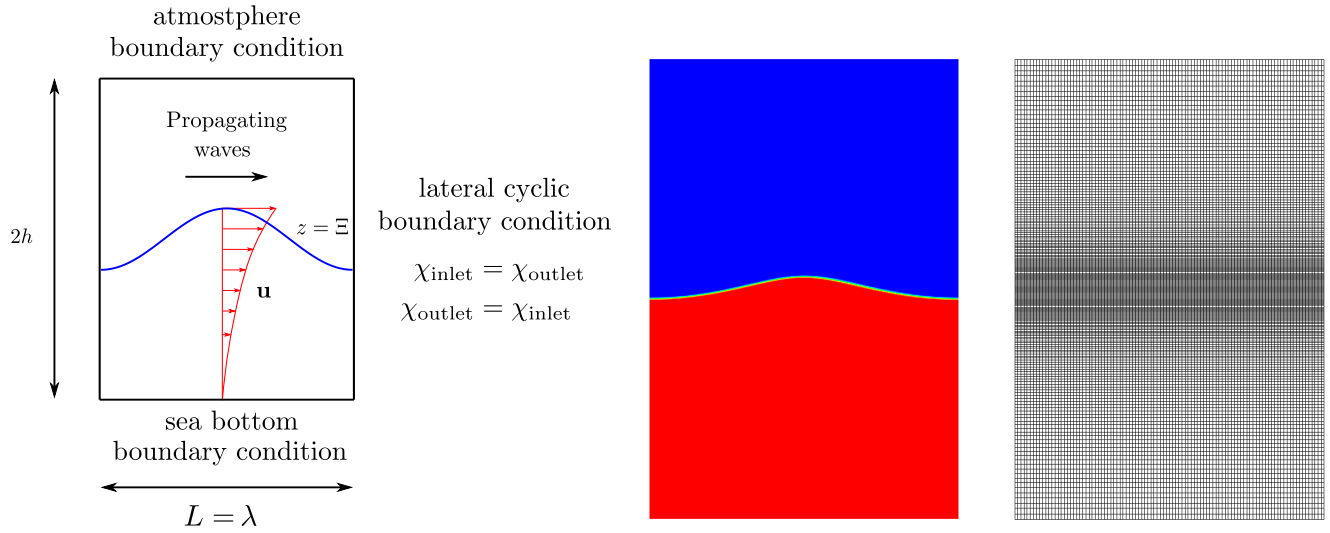


(a) Computational domain (b) Initialized $\alpha$-field (c) Computational mesh

Figure 2. Schematic view on the parametric study of propagating waves with the periodic boundary condition.

Table 1. Wave condition

| Item | Unit | Value |
|---|---|---|
| Water depth ($h$) | [m] | 0.6 |
| Wave period ($T$) | [s] | 0.7018 |
| Wave height ($H$) | [m] | 0.0575 |
| Wavelength ($\lambda$) | [m] | 0.8082 |
| $H/\lambda$ | [-] | 0.0712 |

The parametric study on spatial and temporal discretization is conducted with parameters in Table 2. Representative Courant (Co) and Reynolds numbers ($\text{Re}_\Delta$) are kept in a set of simulations and they are given in

$$\text{Co} = \sqrt{\text{Co}_x^2 + \text{Co}_z^2}, \qquad \text{Re}_\Delta = \sqrt{\text{Re}_{\Delta x}^2 + \text{Re}_{\Delta z}^2} \tag{29}$$

with

$$\text{Co}_x = \frac{u_{\text{wave}}\Delta t}{\Delta x}, \quad \text{Co}_z = \frac{w_{\text{wave}}\Delta t}{\Delta z}, \quad \text{Re}_{\Delta x} = \frac{u_{\text{wave}}\Delta x}{\nu_w}, \quad \text{Re}_{\Delta z} = \frac{w_{\text{wave}}\Delta z}{\nu_w}$$

where $u_{\text{wave}}$ and $v_{\text{wave}}$ are the horizontal and vertical fluid velocities obtained from the potential flow model. A Crank-Nicholson time scheme with $c_{CN} = 0.95$ is used for all local terms. Convection terms of complementary LS function transport equation are discretized by `vanLeer` scheme and a first-order upwind scheme is used

Table 2. Spatial and temporal discretization for convergence test.

| **Case** | $\lambda/\Delta x$ | $H/\Delta z$ | $T/\Delta t$ | Co | $\mathrm{Re}_\Delta$ |
|---|---|---|---|---|---|
| Mesh025-dt100 | 25 | 5 | 100 | 0.171 | 8,836 |
| Mesh030-dt120 | 30 | 6 | 120 | 0.171 | 7,363 |
| Mesh040-dt160 | 40 | 8 | 160 | 0.171 | 5,523 |
| Mesh050-dt200 | 50 | 10 | 200 | 0.171 | 4,418 |
| Mesh100-dt400 | 100 | 20 | 400 | 0.171 | 2,209 |
| Mesh200-dt800 | 200 | 40 | 800 | 0.171 | 1,105 |
| Mesh100-dt200 | 100 | 20 | 200 | 0.684 | 2,209 |
| Mesh100-dt800 | 100 | 20 | 800 | 0.086 | 2,209 |
| Mesh100-dt1600 | 100 | 20 | 1600 | 0.043 | 2,209 |

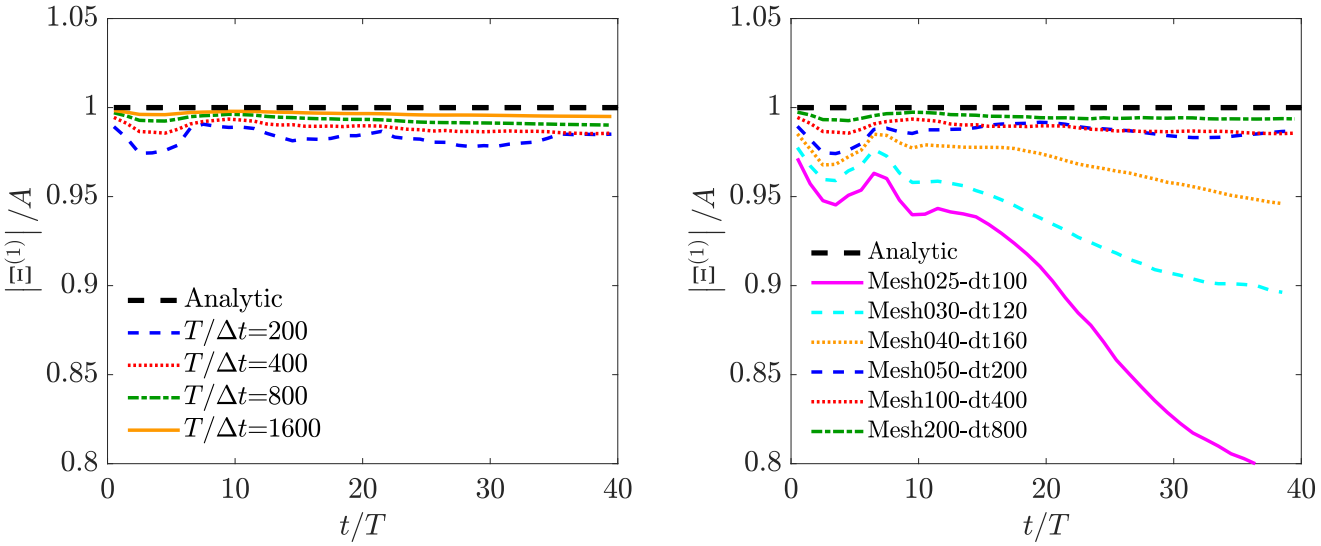


(a) Co discretization

(b) $\mathrm{Re}_\Delta$ discretization

Figure 3. First-harmonic wave amplitudes with respect to Co and $\mathrm{Re}_\Delta$ discretization.

to discretize convection terms in momentum equations. The wave elevation at the center of the computation domain is measured during the simulation. The moving window Fast Fourier Transform (mwFFT) with unit window function over one wave period is applied to obtain the first-harmonic amplitude of wave elevation over simulation time. The first-harmonic amplitudes of wave elevation with respect to Co and $Re_\Delta$ discretizations are shown in Figure 3. When the coarse temporal and spatial discretization are used, the first-harmonic amplitudes of wave elevation show unstable results compared to the simulation case with a fine discretization. The results are convergent to the reference value as fine discretization is applied. The least square procedure of [24] is applied to estimate the order of convergence ($p$) over the observation window $t \in [25T, 40T]$ and the results are shown in Figure 4. The obtained convergence orders for Co and $\mathrm{Re}_\Delta$ discretization are $p = 1.2$ and 2.0, respectively.

The parametric study case is simulated with the other viscous flow solver called `foamStar` with the same discretization. The `foamStar` is viscous flow model solving the Navier-Stokes equations with VOF interface modeling described in [25]. The VOF compression parameter $c_\alpha = 0.3$ used in VOF transport equation is adopted. The first-harmonic amplitudes and phase disturbance during simulation time are compared in Figure 5. The results show that the proposed method based on the SWENSE with LS preserves the propagating waves better than the viscous flow model solving the Navier-Stokes equations with VOF.

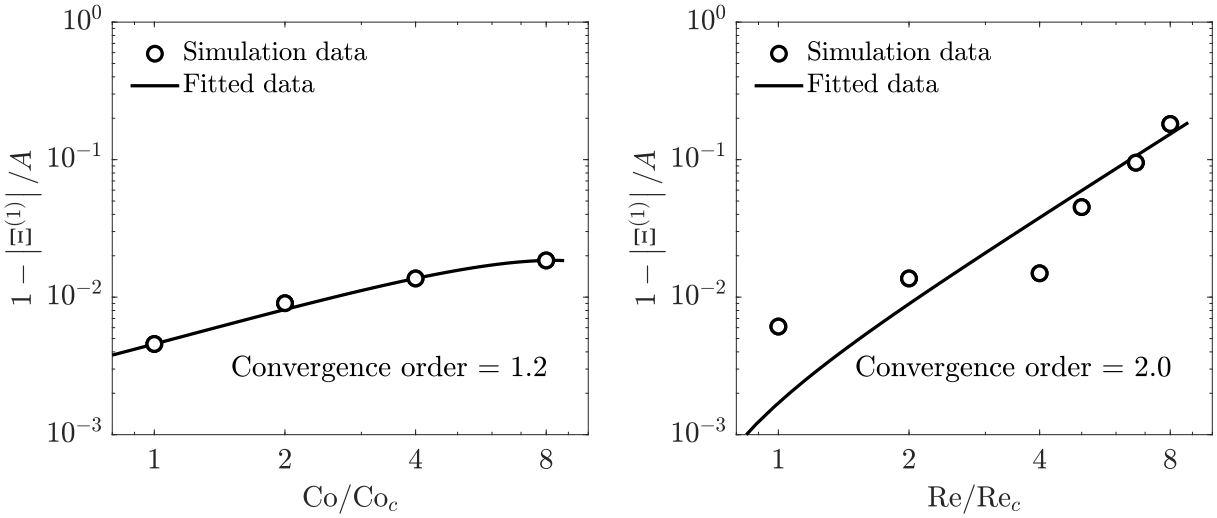


(a) Co discretization (b) $\mathrm{Re}_\Delta$ discretization

Figure 4. The convergence of the first-harmonic amplitude with respect to Co and $\mathrm{Re}_\Delta$ discretizations.

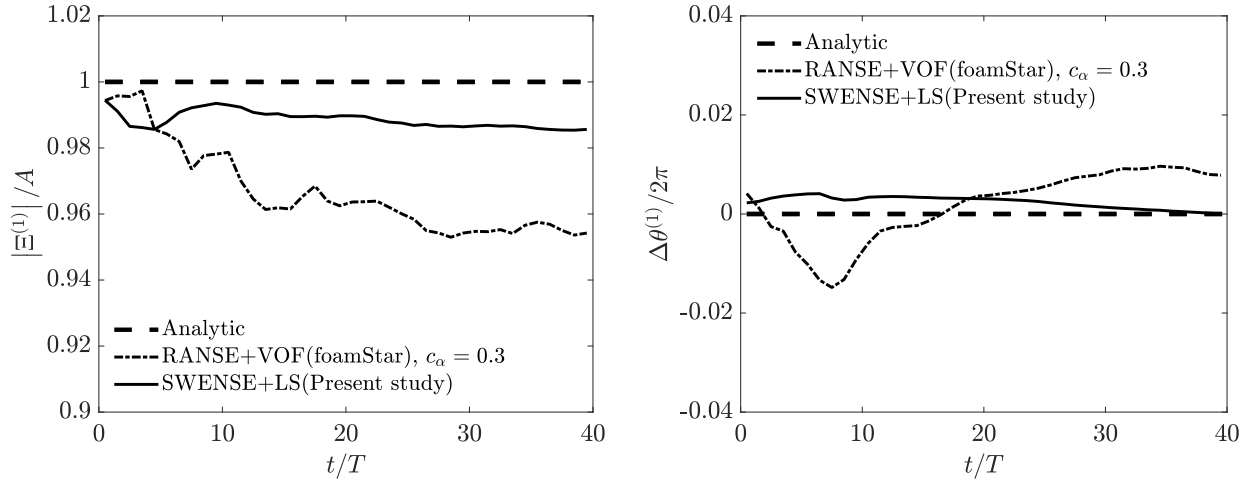


(a) Amplitude (b) Phase difference

Figure 5. Comparison between SWENS equations with LS function and Navier-Stokes equations with VOF for wave propagation.

## 4.2 Force harmonics on the vertical circular cylinder

A benchmark test on a vertical circular cylinder in regular waves is considered. A set of experiments was conducted by [26] to obtain the force harmonics. A cylinder with radius $r = 0.03m$ is fixed in the wave tank of depth $h = 0.6m$. The regular waves of frequency $f = \frac{\omega}{2\pi} = 1.425$ Hz with various wave heights ($H$) are generated in the wave tank. In the present study, simulations are conducted in a wave steepness range $kH \in [0.12, 0.48]$. A circular cylindrical mesh with a radius of $2\lambda = 1.537m$ and the height $0.8m$ is considered. A relaxation zone with the length of $1.5\lambda$ is defined from the outer boundary. The computational domain is discretized with a cell length ratio in the radial direction $\Delta R_{\max}/\Delta R_{\min} = 40$. The number of cells in the radial direction is $N_R = 40$. The mesh is discretized uniformly in $\theta$-direction with $N_\theta = 30$. Three mesh blocks are considered in the vertical direction. The underwater block is defined in $z \in [-0.6H, -0.75H]$ with cell height ratio $\Delta z_{\max}/\Delta z_{\min} = 50$, and number of cells $N_{z1} = 25$ is used. The free surface block is defined in $z \in [-0.75H, 0.75H]$. This part of the domain is discretized uniformly with $N_{z2} = 40$. The air block is defined in $z \in [0.75H, 0.2m]$. Here the mesh uses a cell height ratio $\Delta z_{\max}/\Delta z_{\min} = 12$ with number of cells $N_{z3} = 15$. The computational mesh used for the simulation case $kH = 0.48$ is shown in Figure 6. The time step is set to

$T/\Delta t = 800$. Total number of cells used for computation is $N_{cell} = 190,000$.

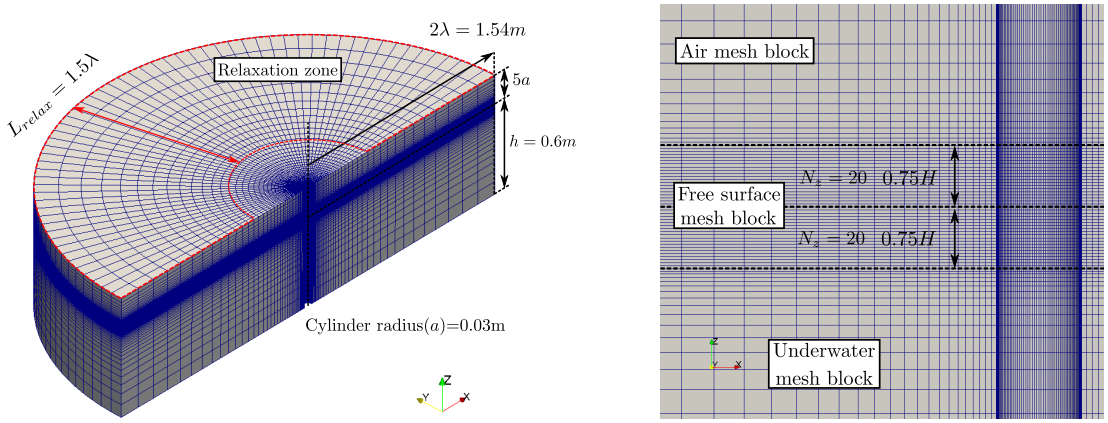


Figure 6. Computational mesh used for thin cylinder in regular waves, $kH = 0.48$.

Figure 7 shows total wave elevations around cylinder for simulation time. Complementary waves generated by a vertical cylinder are clearly verified.

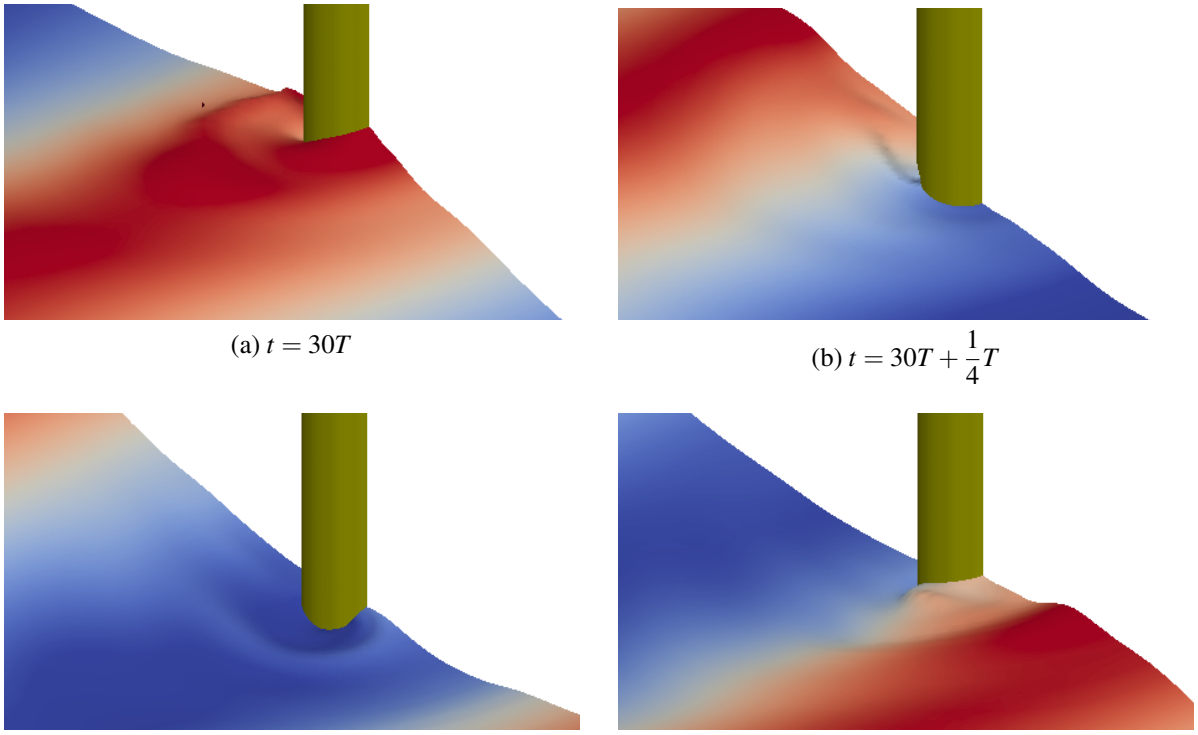

(a) $t = 30T$ (b) $t = 30T + \frac{1}{4}T$

(c) $t = 30T + \frac{2}{4}T$ (d) $t = 30T + \frac{3}{4}T$

Figure 7. Total wave field around cylinder at 4 instants, $kH = 0.48$.

Analytical solutions on the vertical circular cylinder in regular waves are available up to third-order [27, 28, 29]. Amplitudes of force harmonics are normalized as:

$$\frac{\left|F^{(n)}\right|}{\rho_w g r^3}\left(\frac{r}{H/2}\right)^n \tag{30}$$

where $^{(n)}$ denotes the order of harmonics. The phase of force harmonics are denoted as $\vartheta(F_x^{(n)})$ in Figure 8. Obtained first and higher harmonics of horizontal force are compared in Figure 8 with results of associated studies [30, 31, 12].

First-harmonic amplitudes and phases have similar tendencies with the results of [12]. However, small amplitude differences are observed for small $kH$ that should have a similar value with the analytical solution. It is understood that the discretization considered in the present study is not enough to model the small-amplitude waves. Second-harmonic amplitudes and phases show similar results with [12]. Third-harmonic amplitudes and phases are slightly different for small $kH$ compared to others and analytic solution. Force harmonics calculated by the proposed method show good results even though a relative coarse discretization ($N_{cell} = 190,000$) is used.

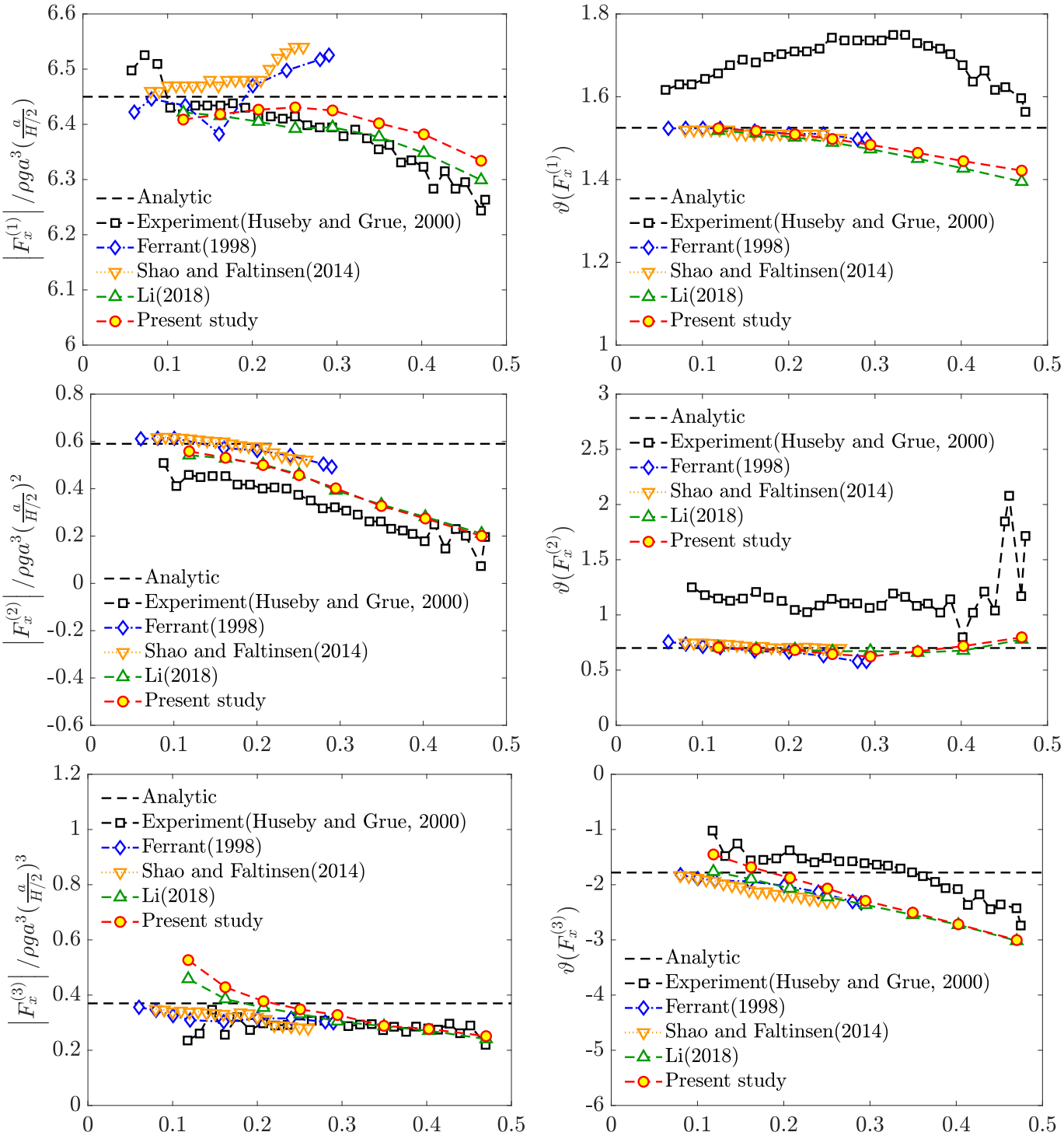


Figure 8. Harmonics of horizontal force acting on the cylinder.

## 5. Conclusion

A SWENSE method based on Level-Set function is proposed for multi-phase flows. The solver is developed in OpenFOAM framework. The fluid velocity, pressure and Level-Set function are decomposed into incident and complementary parts. A parametric study on the temporal and spatial discretization shows good and convergent results to the reference value. On the wave-structure interaction problem chosen, the force-harmonics on the vertical circular cylinder in regular waves show a similar accuracy to associated studies, and this with a relatively coarse spatial and temporal discretization. Further work is needed to assess the performances of the developed solver in a wider range of applications and its competitivity against other solvers.

## Acknowledgement

This work has been performed in the framework of the Chaire Hydrodynamique et Structures Marines Centrale Nantes - Bureau Veritas.

## References

[1] C. W. Hirt and B. D. Nichols, "Volume of fluid (VOF) method for the dynamics of free boundaries," *Journal of Computational Physics*, vol. 39, pp. 201–225, 1981.

[2] S. Osher and J. A. Sethian, "Fronts propagating with curvature-dependent speed: Algorithms based on Hamilton-Jacobi formulations," *Journal of Computational Physics*, vol. 79, no. 1, pp. 12 – 49, 1988.

[3] W. Boettinger, J. Warren, C. Beckermann, and A. Karma, "Phase-field simulation of solidification 1," *Annu. Rev. Mater. Res*, vol. 32, pp. 163–94, 08 2002.

[4] J. P. Boris and D. L. Book, "Flux-corrected transport. I. SHASTA, a fluid transport algorithm that works," *Journal of Computational Physics*, vol. 11, no. 1, pp. 38 – 69, 1973.

[5] A. Di Mascio, R. Broglia, and R. Muscari, "On the application of the single-phase level set method to naval hydrodynamic flows," *Computers & Fluids*, vol. 36, no. 5, pp. 868 – 886, 2007.

[6] J. Roenby, H. Bredmose, and H. Jasak, "A computational method for sharp interface advection," *Royal Society Open Science*, vol. 3, no. 11, 2016.

[7] P. Ferrant, L. Gentaz, B. Alessandrini, and D. Le Touzé, "A potential/RANSE approach for regular water wave diffraction about 2-D structures," *Ship Technology Research*, vol. 50, no. 4, pp. 165–171, 2003.

[8] R. Luquet, B. Alessandrini, P. Ferrant, and L. Gentaz, "RANSE analysis of 2D flow about a submerged body using explicit incident wave models," in *NUmerical Towing Tank Symposium (NUTTS Symposium)*, 10 2003.

[9] L. Gentaz, R. Luquet, B. Alessandrini, and P. Ferrant, "Numerical simulation of the 3D viscous flow around a vertical cylinder in non-linear waves using an explicit incident wave model," in *23rd Int. C. on Offshore Mechanics and Arctic Eng., OMAE2004-51098*, 2004.

[10] C. Monroy, G. Ducrozet, F. Bonnefoy, A. Babarit, L. Gentaz, and P. Ferrant, "RANS simulations of a calm buoy in regular and irregular seas using the SWENSE method," *International Journal of Offshore and Polar Engineering*, vol. 21, 12 2011.

[11] V. Vukčević, H. Jasak, and Šime Malenica, "Decomposition model for naval hydrodynamic applications, part i: Computational method," *Ocean Engineering*, vol. 121, pp. 37 – 46, 2016.

[12] Z. Li, *Two-phase spectral wave explicit Navier-Stokes equations method for wave-structure interactions*. PhD thesis, École Centrale de Nantes, 2018.

[13] M. Kang, R. P. Fedkiw, and X. D. Liu, "A boundary condition capturing method for multiphase incompressible flow," *Journal of Scientific Computing*, vol. 15, no. 3, pp. 323–360, 2000.

[14] K. Y. Lervåg, *Simulation of two-phase flow with varying surface tension*. PhD thesis, Norwegian University of Science and Technology (NTNU), 2008.

[15] J. Huang, P. M. Carrica, and F. Stern, "Coupled ghost fluid/two-phase level set method for curvilinear body-fitted grids," *International Journal for Numerical Methods in Fluids*, vol. 55, no. 9, pp. 867–897, 2007.

[16] N. G. Jacobsen, D. R. Fuhrman, and J. Fredsøe, "A wave generation toolbox for the open-source CFD library: OpenFoam®," *International Journal for Numerical Methods in Fluids*, vol. 70, no. 9, pp. 1073–1088, 2012.

[17] M. M. Rienecker and J. D. Fenton, "A Fourier approximation method for steady water waves," *Journal of Fluid Mechanics*, vol. 104, p. 119–137, 1981.

[18] G. Ducrozet, B. Bouscasse, M. Gouin, P. Ferrant, and F. Bonnefoy, "CN-Stream: Open-source library for nonlinear regular waves using stream function theory," *arXiv:1901.10577 [physics.flu-dyn]*, 2019.

[19] S. Seng, *Slamming and whipping analysis of ships*. PhD thesis, Technical University of Denmark (DTU), Lyngby, 2012.

[20] V. Vukčević, *Numerical modelling of coupled potential and viscous flow for marine applications*. PhD thesis, University of Zagreb, 2016.

[21] H. Jasak, *Error analysis and estimation for the finite volume method with applications to fluids flows*. PhD thesis, Imperial College, 1996.

[22] H. Rusche, *Computational fluid dynamics of dispersed two-phase flows at high phase fractions*. PhD thesis, Imperial College, 2002.

[23] Y.-M. Choi, Y. J. Kim, B. Bouscasse, S. Seng, L. Gentaz, and P. Ferrant, "Performance of different techniques of generation and absorption of free-surface waves in computational fluid dynamics," *Ocean Engineering*, vol. 214, p. 107575, 2020.

[24] L. Eça and M. Hoekstra, "A procedure for the estimation of the numerical uncertainty of CFD calculations based on grid refinement studies," *J. of Comp. Physics*, vol. 262, pp. 104 – 130, 2014.

[25] C. Monroy and S. Seng, "Time-stepping schemes for seakeeping in openfoam," 11 2017.

[26] M. Huseby and J. Grue, "An experimental investigation of higher-harmonic wave forces on a vertical cylinder," *Journal of Fluid Mechanics*, vol. 414, p. 75–103, 2000.

[27] R. C. McCamy and R. A. Fuchs, "Wave forces on piles: A diffraction theory," 1954. Tech. Memo No. 69, U.S. Army Corps of Engrs.

[28] M.-H. Kim and D. K. P. Yue, "The complete second-order diffraction solution for an axisymmetric body Part 1. Monochromatic incident waves," *Journal of Fluid Mechanics*, vol. 200, p. 235–264, 1989.

[29] Š. Malenica and B. Molin, "Third-harmonic wave diffraction by a vertical cylinder," *Journal of Fluid Mechanics*, vol. 302, p. 203–229, 1995.

[30] P. Ferrant, "Fully nonlinear interactions of long-crested wave packets with a three dimensional body," in *Proc. 22nd ONR symposium on Naval Hydrodynamics*, pp. 403–415, 1998.

[31] Y.-L. Shao and O. M. Faltinsen, "A harmonic polynomial cell (HPC) method for 3D Laplace equation with application in marine hydrodynamics," *Journal of Computational Physics*, vol. 274, pp. 312 – 332, 2014.